

Geochemistry, Geophysics, Geosystems®



RESEARCH ARTICLE

10.1029/2023GC011325

Key Points:

- The last magnetic reversal at Scotia Sea Site U1538 is offset downward by ~20 m compared to the more reliable Site U1537 record
- Ferrous iron enrichment below the sulfate reduction depth is observed at Site U1538
- Anomalous magnetic minerals and porewater differences reveal a geochemical setting conducive to chemical remanent magnetization acquisition

Correspondence to:

B. T. Reilly,
breilly@ldeo.columbia.edu











Citation:

Reilly, B. T., Tauxe, L., Brachfeld, S. A., Kenlee, B., Gutjahr, M., Dale, A. W., et al. (2024). A geochemical mechanism for >10 m apparent downward offsets of magnetic reversals inferred from comparison of two Scotia Sea drill sites. *Geochemistry, Geophysics, Geosystems*, 25, e2023GC011325. <https://doi.org/10.1029/2023GC011325>

Received 2 NOV 2023

Accepted 2 JUL 2024

A Geochemical Mechanism for >10 m Apparent Downward Offsets of Magnetic Reversals Inferred From Comparison of Two Scotia Sea Drill Sites

Brendan T. Reilly¹ , Lisa Tauxe² , Stefanie A. Brachfeld³ , Bridget Kenlee⁴, Marcus Gutjahr⁵ , Andrew W. Dale⁵ , Iván Hernández-Almeida⁶ , Sidney Hemming¹, Ian Bailey⁷ , Xufeng Zheng⁸ , Daven Cheu², Reece Taglienti², Michael E. Weber⁹ , Maureen E. Raymo¹ , and Trevor Williams¹⁰

¹Lamont-Doherty Earth Observatory, Columbia University, Palisades, NY, USA, ²Scripps Institution of Oceanography, University of California San Diego, La Jolla, CA, USA, ³Earth and Environmental Studies, Montclair State University, Upper Montclair, NJ, USA, ⁴Crowder College, Neosho, MO, USA, ⁵GEOMAR Helmholtz Centre for Ocean Research Kiel, Kiel, Germany, ⁶Past Global Changes, University of Bern, Bern, Switzerland, ⁷Camborne School of Mines, University of Exeter, Cornwall, UK, ⁸South China Sea Institute of Oceanology, Chinese Academy of Sciences, Guangzhou, China, ⁹Institute for Geosciences, University of Bonn, Bonn, Germany, ¹⁰International Ocean Discovery Program, Texas AM University, College Station, TX, USA

Abstract We document an apparent downward displacement of the Matuyama-Brunhes magnetic reversal by ~20 m at Scotia Sea International Ocean Discovery Program Site U1538 (Pirie Basin) by comparison with the well-defined paleomagnetic record at nearby Site U1537 (Dove Basin). Detailed stratigraphic correlation between the two sites is possible due to similar lithologic variations. However, the two sites have distinctly different porewater geochemistry. Notably, Site U1538 indicates a greater demand for electron acceptors to oxidize organic carbon and Fe²⁺ enrichment below the depth of SO₄²⁻ depletion. Magnetic parameters indicate enrichment of an authigenic magnetic mineral with strong remanence properties around the depth of SO₄²⁻ depletion (~46 m at Site U1538) relative to magnetic parameters at correlative depths at Site U1537. Fe²⁺ enrichment below the depth of SO₄²⁻ depletion is not predicted based on the energetically favorable order of electron acceptors for microbial respiration but is documented here and in other depositional settings. This indicates Fe²⁺ production exceeds the production of H₂S by SO₄²⁻ reduction, providing a geochemical environment that favors the production and preservation of ferrimagnetic remanence-bearing iron sulfides over paramagnetic pyrite and, thus, a mechanism for deep chemical remanent magnetization acquisition at depths of tens of meters. The influence of authigenic ferrimagnetic iron sulfides on paleomagnetic signals can be difficult to demonstrate with magnetic properties alone; therefore, this finding has implications for evaluating the fidelity of magnetostratigraphic records with complementary geochemical data. Such situations should be considered in other depositional environments with similar porewater Fe²⁺ accumulation below the SO₄²⁻ reduction depth.

Plain Language Summary Sediment on the seafloor is an archive of Earth history, including past climate variations, ice sheet dynamics, and geomagnetic field variations. The lattermost include a history of when the Earth's magnetic field flipped upside down in the past so that compass needles would have pointed to the South Pole instead of the North Pole. Scientists have a good understanding of when these flips happened and, once identified in sedimentary layers, the flips can be used to identify time horizons—which are useful for dating other events recorded by the sediment. In this study, we present two magnetic reconstructions from nearby locations that initially recorded the same geomagnetic signals. After deposition, one of the magnetic records changed as a result of chemical reactions that modified the magnetic minerals in the sediment, making it difficult to correlate to the geomagnetic time scale. We have a nearby record with minimal chemical modifications so we could identify the chemical reactions were likely responsible for the changes. This observation will provide additional insights into what signals to look for when studying similar complications from other locations in the world.

1. Introduction

Sedimentary magnetic mineral assemblages are a reflection of sediment provenance, sediment transport, and diagenetic alteration (Q. Liu et al., 2012). The latter can result in the dissolution of iron oxides like magnetite and/

© 2024 The Author(s). Geochemistry, Geophysics, Geosystems published by Wiley Periodicals LLC on behalf of American Geophysical Union.

This is an open access article under the terms of the [Creative Commons Attribution License](https://creativecommons.org/licenses/by/4.0/), which permits use, distribution and reproduction in any medium, provided the original work is properly cited.

or growth of authigenic minerals including ferrimagnetic iron sulfides like greigite and hexagonal 3C pyrrhotite (Hornig, 2018; Karlin & Levi, 1983; Roberts, 2015). Numerous complex factors control the depths at which authigenic ferrimagnetic iron sulfides form (Roberts, 2015). The offset between the sediment-water interface and the depth of ferrimagnetic sulfide formation can make the measured paleomagnetic signal recorded by the chemical remanent magnetization (CRM) appear older than the stratigraphic horizon in which they are found. In some settings, relatively deep formation is indicated, which could complicate polarity interpretations (Jiang et al., 2001) and smooth paleomagnetic signals (Rowan et al., 2009), while in other settings, minimal offset is observed due to shallow greigite formation that would minimally impact or even improve the recording of paleomagnetic signals (Blanchet et al., 2009; Ebert et al., 2021; Reynolds et al., 1999). It is likely that several geochemical scenarios exist in which ferrimagnetic iron sulfides can form that could result in small, large, and/or multiple generations of offsets in the depth of the CRM relative to the primary depositional remanent magnetization (DRM) (Fu et al., 2008; Roberts & Weaver, 2005).

Magnetic mineral authigenesis is largely controlled by porewater geochemistry, particularly through the production of dissolved Fe^{2+} during Fe^{3+} reduction and the production of H_2S during SO_4^{2-} reduction (Amiel et al., 2020; Berner, 1984; Canfield & Berner, 1987; Karlin & Levi, 1983; Reilly et al., 2020). The order in which electron acceptors are used in microbial respiration is governed by their energetic favorability (Froelich et al., 1979), with Fe^{3+} being more energetically favorable than SO_4^{2-} . In traditional diagenetic models, Fe^{2+} accumulates in porewaters at the depth range of Fe^{3+} reduction and is consumed by upward H_2S diffusion from deeper SO_4^{2-} reduction to create iron sulfides like pyrite. However, in nature, there are mechanisms by which Fe^{3+} can also be used as an electron acceptor at greater depths, such as the proposed anaerobic oxidation of methane coupled with iron reduction (Beal et al., 2009; Chuang et al., 2021; Riedinger et al., 2014), in which Fe^{2+} can accumulate below the SO_4^{2-} reduction zone. These mechanism and others can result in a geochemical environment where Fe^{2+} accumulates more rapidly than it can be consumed by H_2S , creating conditions that favor precipitation and preservation of sulfide-limited iron sulfides, including the ferrimagnetic phases greigite and/or hexagonal 3C pyrrhotite, over pyrite (Blanchet et al., 2009; Hornig, 2018; Hornig & Roberts, 2018; Hunger & Benning, 2007; Kao et al., 2004; Reilly et al., 2020; Roberts et al., 2011; Rowan et al., 2009). Direct comparison of high-resolution porewater geochemistry and magnetic measurements has clearly demonstrated ferrimagnetic enrichment where Fe^{2+} concentrations are enhanced below the SO_4^{2-} reduction zone (Amiel et al., 2020; Reilly et al., 2020).

In 2019, International Ocean Discovery Program (IODP) Expedition 382, *Iceberg Alley and Subantarctic Ice and Ocean Dynamics*, drilled several sites in the Scotia Sea from deep-sea contourite deposits in the Dove and Pirie Basins (Figure 1; Pérez et al., 2021; Weber et al., 2021b). One of the exceptional aspects of these records is the tight relative stratigraphic control made possible between sites due to similar lithologic variability (Bailey et al., 2022; Reilly et al., 2021). In this framework, Dove Basin Sites U1536 (3,220 m) and U1537 (3,713 m) have reproducible, reliable magnetic polarity stratigraphy (Bailey et al., 2022; Reilly et al., 2021; Warnock et al., 2022; Weber et al., 2022); whereas, the initial interpretation of Pirie Basin Site U1538 (3,131 m) inclination data was more ambiguous and indicated apparent normal polarity in sediments that were likely deposited during the reverse Matuyama C1r.1r Chron (Figures 2 and 3; Weber et al., 2021d).

Pirie Basin Site U1538 and Dove Basin Site U1537 have contrasting porewater geochemistry (Weber et al., 2021c, 2021d), which provides a rare opportunity to compare sediment magnetic data from sites with similar lithologic variations but different diagenetic environments, and which are only ~350 km apart. It can be challenging to determine how diagenesis has modified a paleomagnetic signal at a single site using magnetic methods alone, as authigenic ferrimagnetic iron sulfides can have similar magnetic coercivities and properties to other magnetic minerals. Thus, unraveling the factors behind the complicated Site U1538 magnetic signals in the context of Site U1537 variations will offer insight into how the fidelity of magnetostratigraphic records can be evaluated in the context of porewater and sediment geochemistry.

1.1. Shipboard Observations and Motivation

Two stratigraphic lines of evidence conflict with the initial Site U1538 Matuyama-Brunhes boundary pick made during IODP Expedition 382 based on paleomagnetic data alone. First, the last occurrence (LO) of the radiolarian *Pterocanium charybdeum trilobum* (Haeckel, 1861) was unexpectedly identified in an apparent normal polarity zone, immediately above the stable reverse polarity horizon at Site U1538 used to initially define the end of the

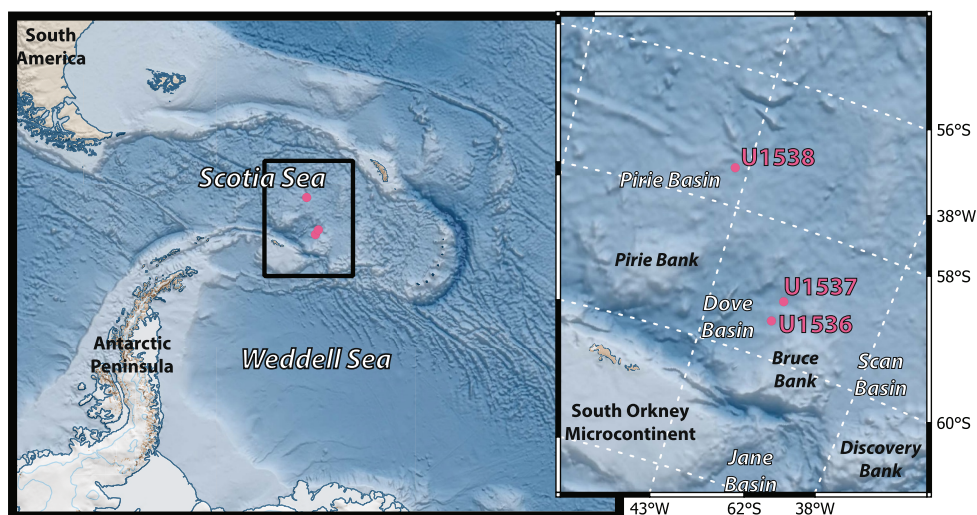


Figure 1. International Ocean Discovery Program drill sites from Dove and Pirie Basins in the Scotia Sea are studied here. Sites U1536 and U1537 (Dove Basin) and Site U1538 (Pirie Basin) sampled deep-sea contourite deposits, for which seismic context is documented by Pérez et al. (2021). Map generated using the Quantarctica QGIS package (Matsuoka et al., 2021) using the IBCSO bathymetry (Arndt et al., 2013).

C1r.1r Matuyama Chron (Figure 2; Weber et al., 2021d). The LO of *P. trilobum* in the Southern Ocean is long known to have occurred during the reverse polarity C1r.1r since the earliest magnetic stratigraphy studies (Hays & Opdyke, 1967; Opdyke et al., 1966), dated at approximately 860 ka (Gradstein et al., 2012). Second, leveraging the markedly similar sediment physical property pattern observed between Dove Basin Sites U1536 and U1537 and Pirie Basin Site U1538 (Figures 3 and 4), Bailey et al. (2022) established the correlation of Site U1538 to the Site U1537 depth scale using natural gamma radiation (NGR), which primarily tracks the abundance of terrigenous sediment derived K , and the b^* blue-yellow color parameter, which has been shown to correlate with biogenic silica concentrations in the Scotia Sea (Sprenk et al., 2013; Weber et al., 2022). This provides a clear stratigraphic correlation of Pleistocene glacial-interglacial lithologic variability between the two sites but suggests that the initial Matuyama-Brunhes boundary pick was apparently displaced ~ 16 – 22 m downward relative to its occurrence in marine isotope stage (MIS) 19 at Site U1537 (Figure 3). Based on the correlation to Site U1537, an extended zone of noisy but apparent normal polarity was present below the expected Matuyama-Brunhes transitional interval, with additional noisy data in the reverse polarity intervals bracketing the Jaramillo C1r.1n Subchron (Figure 3).

While these data indicate that the Site U1538 magnetostratigraphy is not reliable, the magnetic polarity stratigraphy of Site U1537 to which we compare is considered robust (Reilly et al., 2021). High-resolution comparisons of Site U1537 stratigraphy to ice core chronologies for the last 800 kyr place the last magnetic reversal in late MIS 19 (Weber et al., 2022), where the reversal is found in other locations when direct benthic $\delta^{18}\text{O}$ comparisons are possible (Channell et al., 2010; Shackleton & Opdyke, 1973; Tauxe et al., 1996). Additionally, anomalous and reproducible directions that are interpreted as the Iceland Basin event occur at the transition from MIS 7 to MIS 6 at Site U1537, as recognized in both Northern and Southern Hemisphere archives (Figure 4; Channell, 2014; Channell et al., 2017).

Despite the similar lithostratigraphy, the two sites have several notable differences that provide an opportunity to study the factors that might contribute to the less reliable magnetostratigraphy at Site U1538. Accumulation rates are higher at Site U1538, which could be explained by several factors, such as differences in primary productivity and/or sediment focusing factors in these contourite deposits (e.g., Sprenk et al., 2013). Importantly for magnetic minerals, geochemical observations suggest a higher demand on electron acceptors by microbes for organic carbon oxidation at Site U1538 (Figure 2). This demand is manifested as a substantially shallower SO_4^{2-} depletion depth, with SO_4^{2-} concentrations falling below 5% of sea-level concentrations at around 46 m below sea floor (mbsf) at Site U1538 but not until around 80 mbsf at Site U1537. In the upper 250 mbsf, average total organic carbon (TOC) wt.% at Site U1538 is 0.4% versus 0.3% at Site U1537 (Figure 2). Elevated organic matter

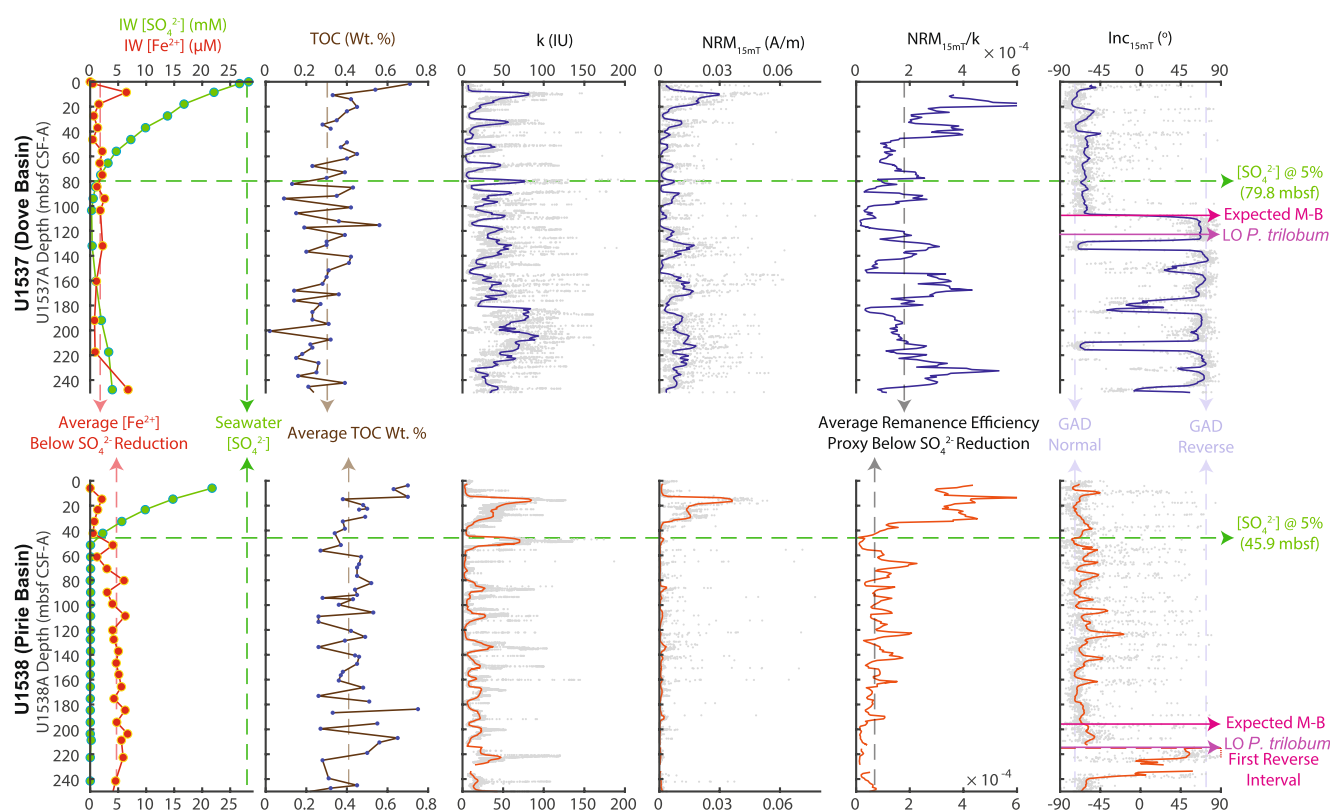


Figure 2. Summary of shipboard geochemical and magnetic data. Shipboard data for the upper 250 m at Holes U1537A (top row; Weber et al., 2021c) and U1538A (bottom row; Weber et al., 2021d). From left to right: interstitial water sulfate (green) and ferrous iron (red). The depth of sulfate reduction (horizontal green dashed line) is nominally calculated where sulfate concentrations are 5% of seawater concentrations (~80 m at U1537A and ~46 m at U1538A). Average ferrous iron concentrations below the sulfate reduction zone (vertical red dashed line) are higher in Hole U1538A than U1537A. Total organic carbon weight % (blue) is also on average higher in Hole U1538A, with variability between samples as a function of variable ooze and silty clay lithology. Magnetic susceptibility (k) and the natural remanent magnetization after 15 mT alternating field (AF) demagnetization (NRM_{15mT}) are plotted as individual measurements (gray dots) and as a 5-m-wide running median (black/red lines). NRM_{15mT}/k of the running median is plotted as a proxy for remanence efficiency, with U1537A having higher values on average below sulfate reduction depths. Inclination after 15 mT AF demagnetization (Inc_{15mT}) with the expected values for a geocentric axial dipole are plotted. The expected Matuyama-Brunhes reversal location is indicated based on assignment of marine isotope stage 19 (Bailey et al., 2022; Weber et al., 2022). The last occurrence of the radiolarian, *P. trilobum*, is also indicated, which is expected to be found in C1r.1r at around 860 ka. Inclination data are all raw, unedited data collected in Hole A at each site, and include ice-rafted debris clasts and disturbed intervals.

degradation at Site U1538 compared to U1537 is also indicated by substantially higher dissolved phosphate and ammonium concentrations in sedimentary interstitial waters (Weber et al., 2021c, 2021d).

Interestingly, neither site has significant porewater dissolved CH_4 concentration at any depth, and thus no clear sulfate-methane transition zone (SMTZ). Average CH_4 concentrations at Sites U1537 and U1538 are 2.3 and 2.9 ppmv, respectively, and there is no concentration trend with respect to depth or SO_4^{2-} concentrations (Weber et al., 2021c, 2021d). For comparison, Site U1534 was studied using the same shipboard methods and drilled on the same expedition to the north at 604 m water depth on the continental slope ~660 km east of the Strait of Magellan. This site had a clearly defined SMTZ with CH_4 concentrations exceeding 50,000 ppmv below the SO_4^{2-} reduction depth (Peck et al., 2021). The lack of dissolved CH_4 at Sites U1537 and U1538 will be explored in future work using geochemical modeling, but may result from a combination of low methanogenesis rates and rapid CH_4 oxidation after production.

SO_4^{2-} reduction produces H_2S , which reacts with Fe^{2+} sourced first from highly reactive iron species and later from crystalline iron forms such as magnetite, which when dissolved combine to produce iron sulfide minerals (Canfield & Berner, 1987). Thus, the H_2S concentration that accumulates in porewaters is a balance between the SO_4^{2-} reduction rate and Fe^{2+} availability with which to react. The H_2S concentration is not measured routinely as part of IODP shipboard protocols, and such data are not available for Expedition 382 records. Higher SO_4^{2-} reduction rates at U1538 and inferred H_2S concentration indicate the potential, however, for greater detrital

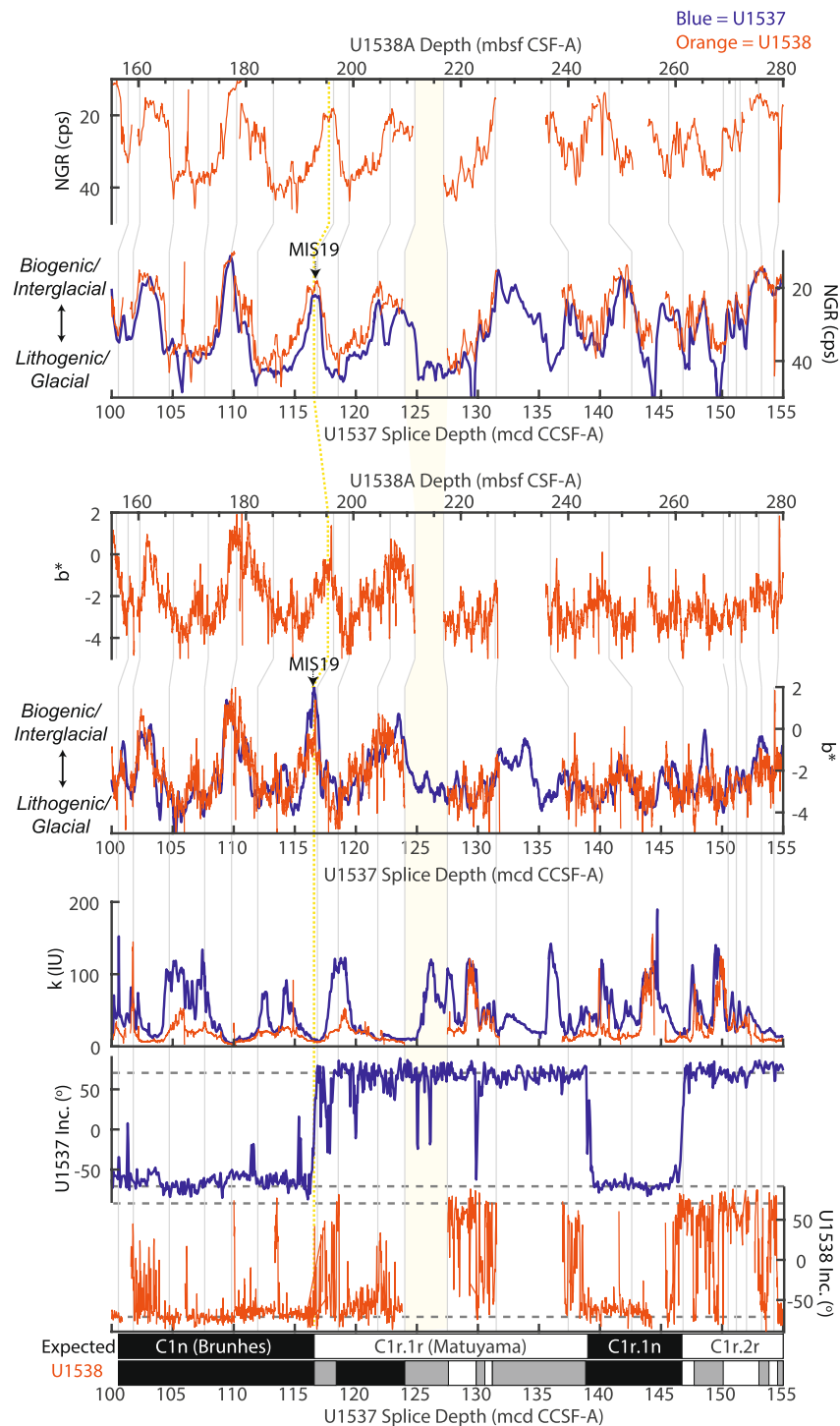


Figure 3. Stratigraphic correlation between sites U1538 and U1537 around the Matuyama-Brunhes reversal. Stratigraphic correlation (gray tie lines) of Bailey et al. (2022) of Hole U1538A (orange) to the Site U1537 splice (blue) based on natural gamma radiation data and supported by b^* reflectance. The location of marine isotope stage 19 is indicated (Weber et al., 2022) along with the location of the Matuyama-Brunhes reversal at Site U1537 (yellow dashed line) and interval of no recovery at Site U1538 for which reverse polarity sediments are below and apparent normal polarity sediments are above (vertical yellow shading). The resulting alignment of down core continuous shipboard magnetic susceptibility (k) and archive half inclination after 15 mT measurements (lower three panels) illustrate the differences between the two sites and ambiguity in interpreting the U1538 paleomagnetic data. The expected inclinations for normal and reverse polarity are indicated with horizontal dashed lines. At the bottom, the expected polarity pattern and an interpretation of the U1538 shipboard archive half polarity pattern are indicated (black = normal; white = reverse; gray = undetermined).

magnetic mineral dissolution and are likely responsible for the larger decrease in magnetic susceptibility (k) and natural remanent magnetization (NRM) intensity at around the SO_4^{2-} reduction depth at Site U1538 relative to Site U1537 (Figure 2). This magnetic mineral diagenesis also has a clear imprint in shipboard data on the paleomagnetic recording potential of sites U1537 and U1538. The ratio of NRM intensity after 15 mT peak alternating field (AF) demagnetization to k ($\text{NRM}_{15\text{mT}}/k$) is a proxy for remanence efficiency (or remanence preservation), and is significantly lower below SO_4^{2-} reduction depths at Site U1538 relative to Site U1537 (Figure 2).

Perhaps the most striking difference from a Fe cycling perspective in the porewater geochemistry of U1537 versus U1538 is that Fe^{2+} is present in concentrations well above the analytical detection limit of the shipboard inductively coupled plasma optical emission spectrometry (i.e., $>\sim 0.5 \mu\text{M Fe}$) below the SO_4^{2-} reduction horizon at Site U1538 (Figure 2). We note that sediment porewater sampling was not conducted under oxygen-free conditions as is usually required for dissolved Fe^{2+} assessment. As a result, in situ dissolved Fe^{2+} concentrations before porewater extraction may have even been higher than shown in Figure 2. While several mechanisms may be responsible for the Fe^{2+} profile shown in Figure 2, the presence of dissolved Fe^{2+} below SO_4^{2-} indicates that its production and/or diffusion rates are greater than its consumption rate by H_2S . This type of geochemical environment, where H_2S is limited with respect to Fe^{2+} , is favorable for authigenic ferrimagnetic iron sulfide formation (Amiel et al., 2020; Kao et al., 2004; Reilly et al., 2020), with the sulfide formation depth most likely at the interface between upward diffusing Fe^{2+} and downward diffusing H_2S near the base of SO_4^{2-} reduction. These conditions occur at approximately 46 mbsf at Site U1538 today, but this sulfide formation depth likely varied through time as environmental conditions changed. For example, as factors such as organic carbon supply, reactive iron supply and sedimentation rate varied, redox zones and key horizons like the SO_4^{2-} reduction depth would migrate vertically in response to increased or decreased microbial demand for electron acceptors.

Site U1538 offers an opportunity to test the potential for deep iron sulfide formation that could be responsible for the apparent downward displacement of magnetic reversals of 10s of meters by comparison of rock magnetic properties with U1537 using the detailed physical properties-based stratigraphic correlation of Bailey et al. (2022; Figures 3 and 4). We consider the Brunhes-Matuyama reversal position at Site U1537 to be the correct stratigraphic horizon and assume that the primary detrital magnetic mineral composition was initially similar at Sites U1537 and U1538. These assumptions are based on the observation that a wide array of shallow Scotia Sea piston cores typically have consistent magnetic variations (Diekmann et al., 2000; Pugh et al., 2009; Weber et al., 2012; Xiao et al., 2016) and that the positions of paleomagnetic reversals at Site U1537 relative to lithologic variations are well reproduced at the higher accumulation rate Dove Basin Site U1536 (Reilly et al., 2021) and are consistent with an independent timescale (Weber et al., 2022). Thus, magnetostratigraphic and mineralogical differences can be considered to be due to diagenetic anomalies at Site U1538.

2. Methods

Vertically oriented paleomagnetic cubes were taken at intervals of ~ 1 per section (~ 1.5 m) in the first drilled hole at Sites U1537 and U1538. While at sea, these cubes were studied to understand the sediment NRM. Nearly all cubes were demagnetized and measured to 15 mT peak AF, while some were demagnetized to higher levels. Shipboard methods and results (along with all other data collected during the expedition) are discussed in the expedition proceedings (Weber et al., 2021a, 2021c, 2021d). Following the expedition, the cube specimens were further studied at the Scripps Institution of Oceanography Paleomagnetic Laboratory. Bulk k was measured on an AGICO KLY-4S Kappabridge and reported values are the mean of three measurements. All remanence measurements were made on a 2G Enterprises three axis superconducting rock magnetometer with direct current Superconducting Quantum Interference Devices. The NRMs were further demagnetized using a static ASC D-2000 AF demagnetizer to measure the remanence before and after demagnetization to peak AFs of 0, 10, 15, 20, 30, 40, 60, 80, and 100 mT (if not previously demagnetized to these levels). Next, anhysteretic remanent magnetizations (ARMs) were imparted using a 100 mT peak AF and 0.05 mT bias field and subsequently demagnetized at 20 and 40 mT peak AF. Finally, isothermal remanent magnetizations (IRMs) were imparted at 100, 300, and 1,000 mT, and then in a -300 mT backfield using an ASC pulse field magnetizer. These data were used to construct a suite of secondary parameters and ratios such as the hard IRM ($\text{HIRM} (\text{IRM}_{1,000\text{mT}} + \text{IRM}_{300\text{mT}})/2$; Robinson, 1986), k_{ARM}/k (Banerjee et al., 1981; King et al., 1982), ARM AF coercivity ratios (e.g., $\text{ARM}_{40\text{mT}}/\text{ARM}$; Peters & Thompson, 1998), IRM ratios (e.g., $\text{IRM}_{100\text{mT}}/\text{IRM}_{300\text{mT}}$), $\text{IRM}_{1,000\text{mT}}$ (SIRM) relative to k (SIRM/k ; Nowaczyk et al., 2013; Snowball & Thompson, 1990), and the S-ratio ($\text{IRM}_{300\text{mT}}/\text{IRM}_{1,000\text{mT}}$; Stober & Thompson, 1979). The potential for gyroremanent magnetization (GRM;

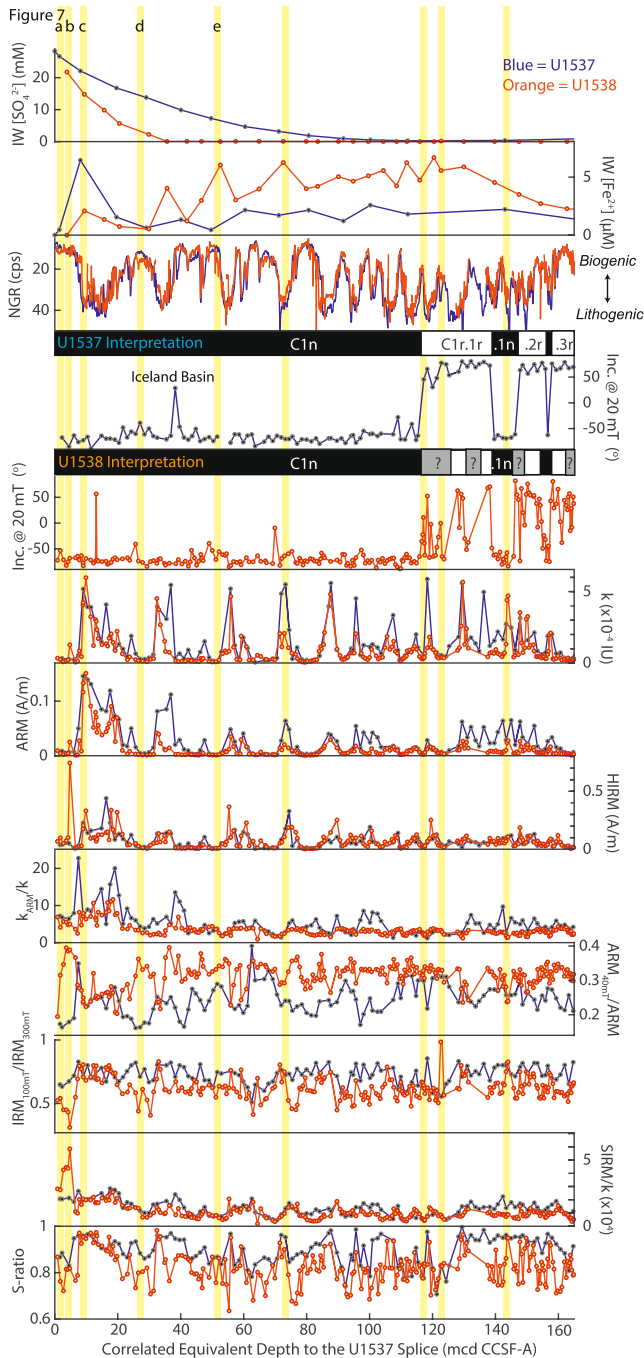


Figure 4.

Stephenson, 1993), the acquisition of magnetic remanence in the plane perpendicular to the last applied AF, is discussed using the $\Delta\text{GRM}/\Delta\text{NRM}$ parameter (Fu et al., 2008). The parameter is slightly modified and calculated as $(\text{NRM}_{@100\text{mT}} - \text{NRM}_{\text{Minimum}})/(\text{NRM}_{\text{Maximum}} - \text{NRM}_{\text{Minimum}})$, as the initial magnetization for sediments with normal magnetization is reduced due to the presence of the nearly antiparallel drill string overprint (see Richter et al., 2007; Weber et al., 2021c, 2021d).

Next, cubes were subsampled and dried sediments were immobilized in an etched borosilicate glass vial with K_2SiO_3 . To investigate the relationship between coercivity and unblocking/alteration temperatures, IRMs were imparted on three axes and were thermally demagnetized at sequentially higher temperatures (Lowrie, 1990). First, a 1,000 mT IRM was imparted along the Z axis. A 300 mT IRM was then imparted along the X axis, and finally a 100 mT IRM was imparted along the Y axis (IRM strengths were selected based on IRMs imparted for initial cube measurements). Specimens were heated in air for 30 min from 100 to 700 at 50°C intervals, cooled to room temperature in a zero field, and measured. For each axis, we calculated the magnetization fraction remaining from the initial magnetization on that axis at 450°C as a proxy for variability in unblocking/alteration temperatures.

Additional rock magnetic measurements were made on a subset of these cubes at the Institute for Rock Magnetism, University of Minnesota. Field cooled (FC), zero field cooled (ZFC), low temperature cycling of room temperature saturation IRM (LTC-SIRM), and alternating current (AC) susceptibility at 1, 10, and 100 Hz were measured on a Quantum Designs Magnetic Properties Measurement System using a 2.5 T field and minimum temperatures of 10 K (see Bilardello & Jackson, 2013). Hysteresis loops, DC demagnetization curves (DCDs), and first-order reversal curves (FORCs) were measured using a Lakeshore 8600 vibrating sample magnetometer. We calculate several parameters from these measurements to capture their variability, including δT_v for FC and ZFC curves $(\text{LTSIRM}_{80\text{K}} - \text{LTSIRM}_{150\text{K}}/\text{LTSIRM}_{80\text{K}})$, where LTSIRM is the FC or ZFC low temperature saturation IRM; Moskowitz et al., 1993), δRTSIRM (change in magnetization before and after LTC-RTSIRM, normalized by the initial RTSIRM), frequency dependent AC susceptibility $(X_{\text{FD}} = (X_{1\text{Hz}} - X_{100\text{Hz}})/X_{1\text{Hz}})$, coercivity of remanence (H_{cr}), and hysteresis loop parameters (e.g., M_r/M_s ; Day et al., 1977). FORC diagrams (Pike et al., 1999; Roberts et al., 2000) were generated using FORCinel v. 3.06 (Harrison & Feinberg, 2008; Harrison et al., 2018) and VARIFORC smoothing (Egli, 2013).

Figure 4. Summary of discrete cube measurements. Discrete cube measurements for Site U1537 (blue) and U1538 (orange) made after the expedition in the context of the interstitial water geochemistry and lithostratigraphy. U1538 data transferred to the U1537 splice depth scale following the correlation of Bailey et al. (2022). Data include: inclination after 20 mT alternating field (AF) demagnetization. Concentration dependent parameters: magnetic susceptibility (k), anhysteretic remanent magnetization (ARM) and HIRM. Concentration independent ratios sensitive to magnetic domain state and mineralogy: anhysteretic susceptibility to k (k_{ARM}/k), ARM after 40 mT AF demagnetization to the original ARM ($\text{ARM}_{40\text{mT}}/\text{ARM}$), isothermal remanent magnetization (IRM) acquired at 100 mT to the IRM acquired at 300 mT ($\text{IRM}_{100\text{mT}}/\text{IRM}_{300\text{mT}}$), saturation IRM acquired at 1,000 mT to k (SIRM/k), and the IRM acquired in a 300 mT backfield to the SIRM (S -ratio). Yellow bars highlight correlative depth intervals investigated with more detailed rock magnetic measurements (Figures 7 and 8), with the letters indicating specimens with the most comprehensive analyses reported in Figure 7 and additional samples including H_{cr} in Figures 8a and 8b.

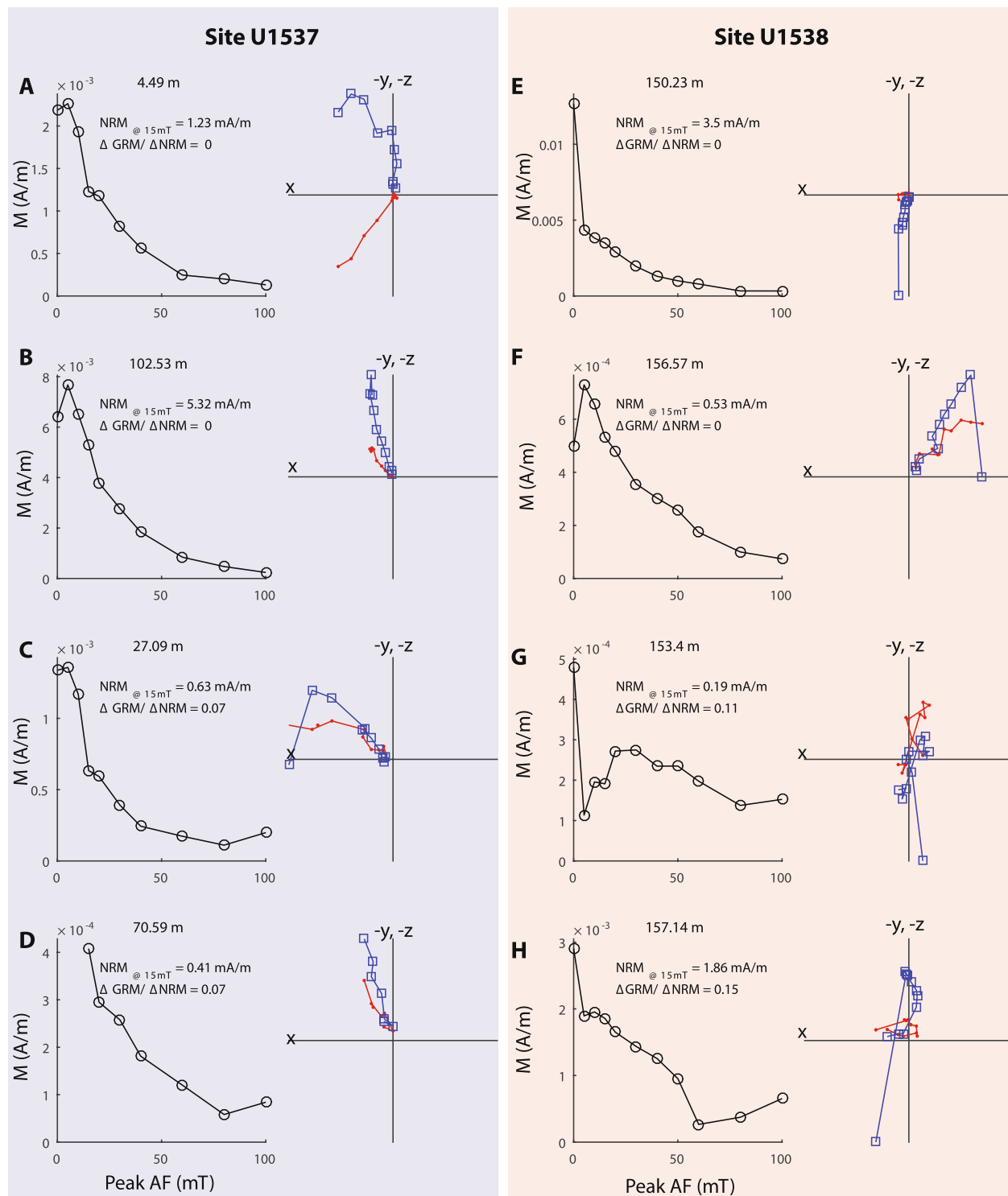


Figure 5. Example alternating field (AF) demagnetization and orthogonal projection plots for well-defined and poorly defined magnetization. Data from Site U1537 (a–d) and Site U1538 (e–h) with sample depth corresponding to the U1537 equivalent depth plotted in Figure 4. Data ≤ 15 mT peak AF were all collected onboard the JOIDES Resolution. Blue open squares represent data projected into the vertical plane, while red closed circles represent data projected in the horizontal plane.

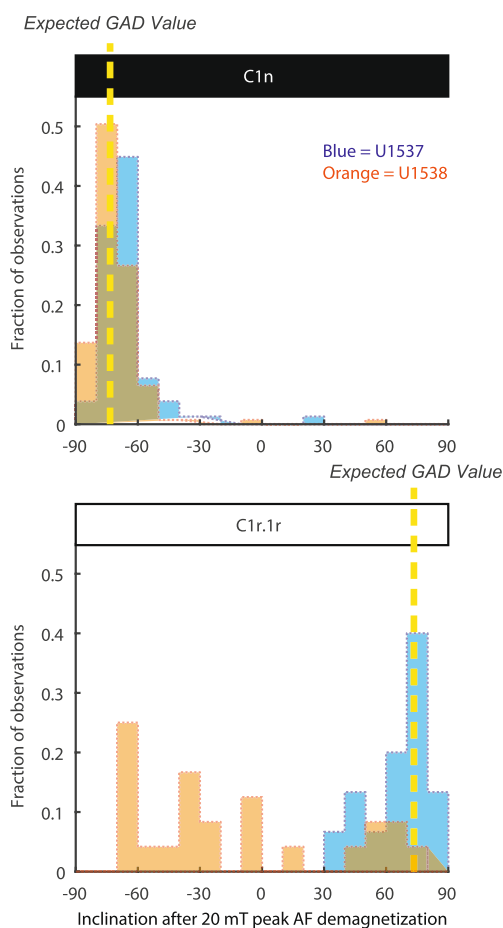


Figure 6. Inclinations histograms. Distributions of inclinations at Site U1537 (blue) and U1538 (orange) during normal polarity Chron C1n and reverse polarity Chron C1r.1r. The expected values based on a geocentric axial dipole for each plot are indicated with a vertical dashed yellow line.

3. Results

3.1. Magnetic Properties

Site U1538 NRM intensities are often weak, particularly below the SO_4^{2-} reduction zone, and are increasingly noisy at higher AF demagnetization steps. In Figure 4, we therefore plot the inclination measured after 20 mT peak AF demagnetization determined post-cruise. These data are largely consistent with the 15 mT peak AF demagnetization data generated shipboard, and are determined following sufficient demagnetization to remove the nearly vertical drill string overprint (Reilly et al., 2021; Weber et al., 2021c, 2021d).

These weak and noisy magnetization at higher AF steps limited our ability to quantify the influence of GRM, such as using the $\Delta\text{GRM}/\Delta\text{NRM}$ parameter of Fu et al. (2008). About 2% of values calculated for Site U1537 in the upper 165 mcd have $\Delta\text{GRM}/\Delta\text{NRM}$ values greater than 0.05 (maximum value = 0.11), while 13% of values calculated for Site U1538 exceed this threshold (maximum value 0.23). However, most of these >0.05 $\Delta\text{GRM}/\Delta\text{NRM}$ values are found in samples from weakly magnetized biogenic lithofacies with NRM intensities <0.002 A/m at Site U1537 and <0.004 A/m at Site U1538. We use demagnetization and orthogonal projection plots (Zijderveld, 1967) in Figure 5 to illustrate examples of demagnetization behavior along with their $\Delta\text{GRM}/\Delta\text{NRM}$ values. For Site U1537, slight intensity increases at high AF steps that lead to $\Delta\text{GRM}/\Delta\text{NRM}$ values >0.5 with no acquisition along the x or y -axis makes it difficult to know if they can be attributed to GRM or to noisy unstable magnetization (Figures 5c and 5d; cf. Figure 3 in Reilly et al., 2021). Some samples from Site U1538 with higher $\Delta\text{GRM}/\Delta\text{NRM}$ values have systematic acquisition at high AF steps consistent with a GRM (Figure 5h), while others with similar $\Delta\text{GRM}/\Delta\text{NRM}$ values have noisy demagnetization behavior, possibly with multiple components, that are challenging to interpret (Figure 5g). Thus, while Site U1538 $\Delta\text{GRM}/\Delta\text{NRM}$ values indicate the potential for greater GRM compared to Site U1537, the underlying explanation is likely a combined influence of GRM and weak unstable magnetization.

The Site U1538 directional data can be further evaluated by a more direct comparison to Site U1537 through the depth transformation of Bailey et al. (2022) to a Site U1537 correlated equivalent depth (ced) (Figures 2 and 3). This comparison shows a mixture of what could be considered normal, intermediate, and reverse polarity directions in C1r.1r. These directions are inconsistent with known stable polarity during C1r.1r and inconsistent with geocentric axial dipole predicted values (Figures 4 and 6).

Concentration dependent parameters measured on the cubes, such as k and ARM, are consistent with shipboard k measurements and indicate that there are often lower concentrations of ferrimagnetic minerals at Site U1538 with respect to Site U1537. In Scotia Sea sediments, k varies strongly on glacial-interglacial timescales, with peaks at Site U1537 during the last 800 kyr corresponding to glacial intervals (Weber et al., 2022). In contrast, HIRM values are fairly similar at the two sites, which suggests the presence of similar high coercivity mineral concentrations that saturate in fields greater than 300 mT. This may not be surprising if the concentrations reflect the degree of dissolution during reductive diagenesis, as it is often observed that hematite is more resistant to dissolution than magnetite (Dillon & Bleil, 2006; Garming et al., 2005; J. Liu et al., 2004; Poulton et al., 2004; Reilly et al., 2020; Yamazaki et al., 2003). However, we also note a few anomalously high HIRM values in the U1538 stratigraphy without corresponding increases in other concentration dependent parameters, which are reminiscent of horizons with increased authigenic iron sulfide preservation that saturate above 300 mT, such as 3C pyrrhotite (Reilly et al., 2020).

Concentration independent parameters also have differences between Sites U1537 and U1538. This is well captured in ratios that track variability within the range of ferrimagnetic coercivities, such as $\text{ARM}_{40\text{mT}}/\text{ARM}$ and

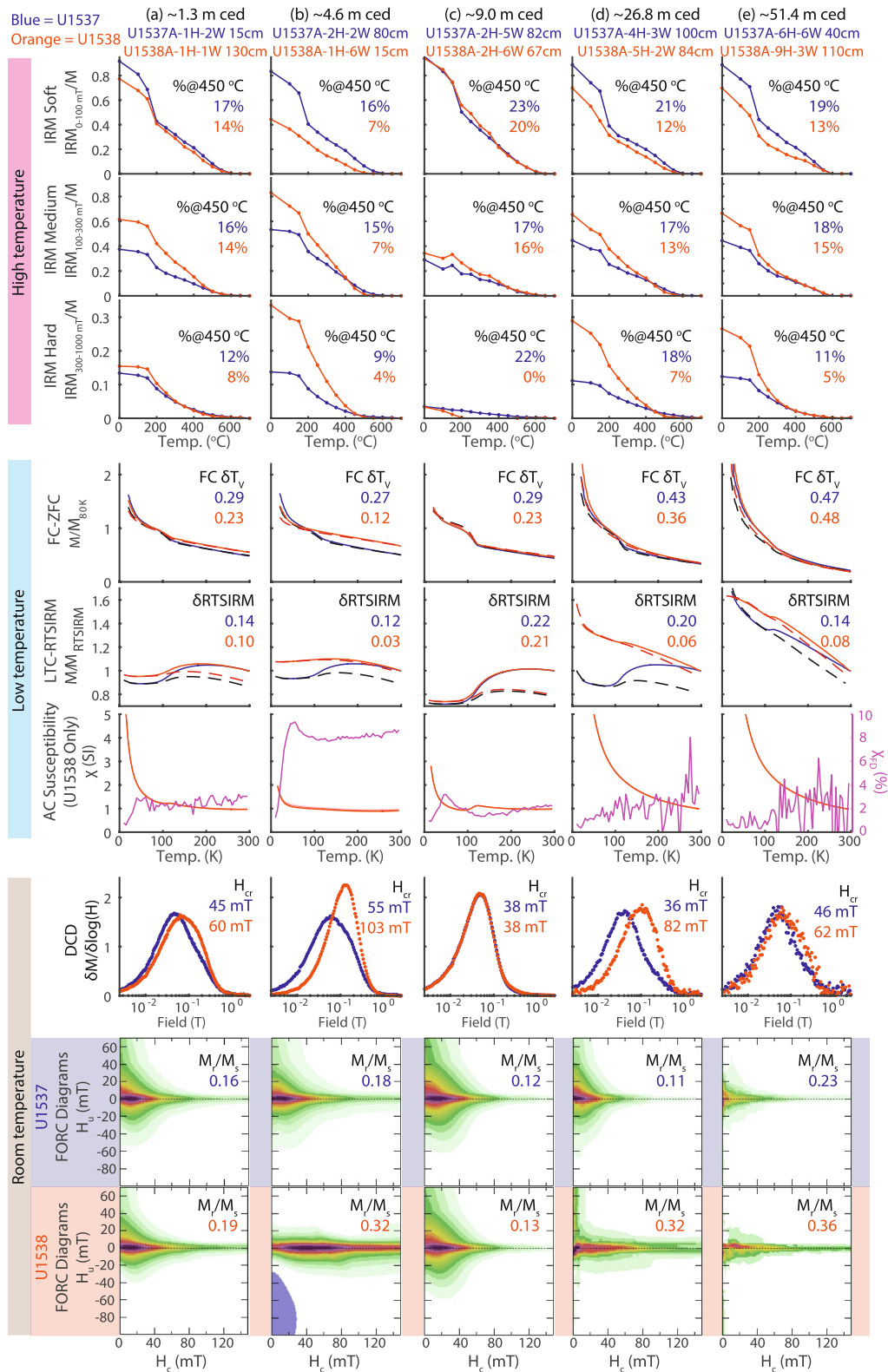


Figure 7.

IRM_{100mT}/IRM_{300mT} (Figure 4). The values of both parameters diverge at the two sites in the upper part of the core in the Holocene interglacial interval (low k , low NGR; 0 to ~ 7 m ced) and then return to similar values during the last glacial interval (high k , high NGR; ~ 7 –19 m ced). Below the last glacial interval (>19 m ced), the values diverge again, with ARM_{40mT}/ARM at Site U1538 remaining fairly constant and high in glacial and interglacial intervals alike (high and low NGR intervals), while U1537 values are generally lower and more variable. The anomalous rock magnetic properties of the Holocene sediments at Site U1538 are unique compared to those before the last glacial interval, with high SIRM/ k values not observed elsewhere, which could be associated with a transient authigenic mineral horizon around the depth of iron reduction characterized by minerals that contribute to the HIRM. S-ratios likely in part reflect preferential magnetite dissolution relative to hematite, as observed in the concentration dependent data (i.e., HIRM is similar at the two sites, while ARM, IRM, and k are reduced at Site U1538).

3.2. Detailed Rock Magnetic Measurements

Detailed rock magnetic data (Figure 7) were collected for select intervals around the depths of modern sulfate reduction to understand magnetic mineralogy variations responsible for the patterns evident from higher resolution data in Figure 4 and to better understand the modern diagenetic environment. The relationship between the higher resolution data collected on the cubes and these additional parameters are summarized in Figure 8. Horizons were chosen to represent (a) the uppermost cube sample taken at each site ~ 1.3 m ced; (b) the equivalent cube samples around the Holocene SIRM/ k peak noted in Figure 4 ~ 4.6 m ced; (c) equivalent cube samples from the last glacial period ~ 9.0 m ced; and (d–e) two equivalent intervals below the SO_4^{2-} reduction depths in U1538 ~ 26.8 and 51.4 m ced. In general, the uppermost sample from each site (Figure 7a) and in the last glacial maximum (Figure 7c) are similar and may be representative of the magnetic properties of the detrital assemblage during interglacial and glacial times, respectively.

Unblocking or alteration temperatures of a three-axis IRM are suppressed at Site U1538 relative to U1537, with less magnetization remaining in all samples and along in soft, medium and hard components by 450°C . The differences between the fraction remaining at 450°C between the two sites are greatest in the ~ 4.6 m ced interval (Figure 7b) and ~ 26.8 m ced interval (Figure 7d). These lower unblocking or alteration temperatures are also associated with suppressed Verwey transitions (T_v in FC and ZFC; and $\delta\text{LTC-RTSIRM}$), with a strong correlation for U1538 samples with $\delta\text{LTC-RTSIRM}$ below ~ 0.1 (Figure 8c). The lowest unblocking or alteration temperatures and most suppressed Verwey transitions are in the U1538 ~ 4.6 m ced sample, which are also characterized by anomalous magnetic properties including high SIRM/ k , HIRM, X_{FD} , and H_{cr} , suggesting relatively high superparamagnetic and high coercivity mineral concentrations (Figures 4 and 7b). FORC diagrams for Site U1537 are consistent with typical observations of detrital magnetic mineral assemblages. Some of the Site U1538 assemblages are similar to their counterparts at Site U1537 (Figures 7a and 7c), while others include an additional component with higher coercivity along the H_c axis and skewed to more negative values along the H_u axis that is not recognized in their counterpart samples at Site U1537 (Figures 7b, 7d, and 7e). This signature is consistent with assemblages that include authigenic iron sulfide phases described elsewhere (Roberts et al., 2018). Overall, there appears to be a strong relationship between coercivity parameters and order-disorder transitions, with U1538 samples generally biased toward higher ferrimagnetic coercivities, more suppressed Verwey transitions, and lower unblocking/alteration temperatures (Figures 7 and 8).

4. Discussion

Despite having similar lithology and stratigraphy, Sites U1537 and U1538 have different magnetic properties. Given the close proximity and similarity of sediment transport pathways to Dove and Pirie Basins, it is unlikely that provenance can explain much of these differences. We argue that the differences are most likely the result of differences in the degree of magnetic mineral diagenesis—both in the dissolution of the primary detrital magnetic

Figure 7. Summary of detailed rock magnetic investigations. Specimens from U1537 (blue) and U1538 (orange) selected from correlative depth intervals were subject to thermal demagnetization of a three-axis 1,000, 300, and 100 mT isothermal remanent magnetization (Lowrie, 1990; normalized to total vector length before thermal demagnetization), FC-ZFC, LTC-RTSIRM, alternating current (AC) susceptibility and frequency dependent AC susceptibility (X and X_{FD} ; U1538 only), direct current demagnetization curves (plotted as the change in magnetization relative to the change in the logarithm of the applied field), and first-order reversal curve diagrams. Columns (a–e) correspond to samples highlighted in Figure 4. Parameters are defined in the methods section.

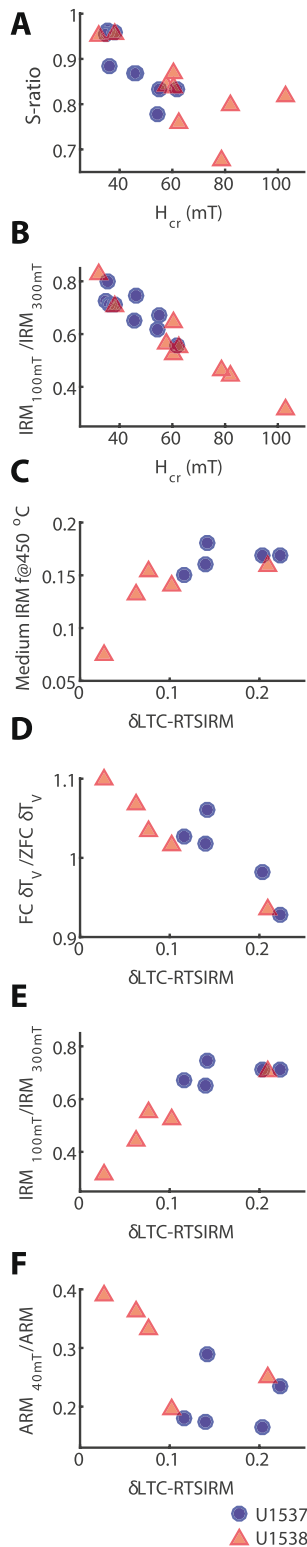


Figure 8. Comparison of detailed rock magnetic properties. Bi-plots of selected rock magnetic parameters to improve interpretation of discrete cube data presented in Figure 4 through comparison to and between the detailed rock magnetic analyses presented in Figure 7. Blue circles are U1537 and orange triangles are U1538.

assemblage and growth of authigenic remanence-bearing iron sulfide minerals. Differences in the growth and preservation of authigenic minerals at the two sites are the most probable explanation for why the U1537 polarity stratigraphy is reliable (Reilly et al., 2021), whereas the U1538 polarity stratigraphy is not. Rock magnetic anomalies at Site U1538 can be described as having (a) suppressed Verwey transitions, (b) lowered unblocking or alteration temperatures, (c) higher ferrimagnetic coercivities, (d) FORC diagrams with distributions skewed to more negative H_u values, and (e) greater superparamagnetic mineral content as indicated by X_{FD} (Figures 4, 7, and 8). These differences between the two sites are all consistent with greater dominance of magnetite (detrital) at Site U1537 and increased influence of remanence-bearing iron sulfides (authigenic) at Site U1538 (Hornig, 2018; Roberts et al., 2011, 2018).

Focusing on the upper ~50 m cored depths at both sites (<80 mbsf on the U1538 actual coring depth), we propose that at least two generations of these authigenic minerals exist. The first formed at shallower depths at Site U1538, above the zone of modern SO_4^{2-} reduction in the low- k and low-NGR Holocene diatom ooze (Figure 4). This interval features some of the most anomalous rock-magnetic properties observed here, but the anomaly appears to be limited to the Holocene and is not found elsewhere in the stratigraphic record—glacial or interglacial (Figure 4). A few thinner horizons with anomalous HIRM and SIRM/ k deeper down core at Site U1538 may exist, but they are rare and, if forming as discrete horizons, may not have been reliably captured in our magnetic data sets due to our ~1.5 m sampling resolution. These high coercivity layers could represent a transient authigenic mineral horizon that forms at a modern redox gradient and is not necessarily well preserved in the stratigraphy, such as well-documented Mn oxide layers (Froelich et al., 1979) or authigenic magnetic minerals (Reilly et al., 2020) that form at different redox horizons. These minerals seem to be limited to Holocene horizons. We do not see any sign of them in the more terrigenous silty clay of the last glacial interval or biogenic ooze of the last interglacial at ~25 m cored (Figures 4 and 7), which suggests either (a) that their formation, but not preservation, is related to a non-steady state diagenetic process that had a greater influence when the biogenic sediment supply was higher in interglacial times, or (b) that this diagenetic signal may be hidden in glacial silty-clay sediments at our study sites because terrigenous inputs are high enough during these times to dilute its influence on bulk magnetic properties.

We propose that a second generation of magnetic minerals forms at greater depths below the SO_4^{2-} reduction interval (>~46 mbsf), where Fe^{2+} is enriched in porewaters at Site U1538. Previous studies have demonstrated that this type of geochemical environment, although not predicted based on traditional early diagenetic models (e.g., Froelich et al., 1979), is associated with ferrimagnetic iron sulfide enrichment when found at shallower depths (Amiel et al., 2020; Reilly et al., 2020). Here, we find that below these depths, ferrimagnetic coercivity diverges between Sites U1537 and U1538, which persist in interglacial and glacial intervals alike (Figure 4). The higher coercivities at Site U1538 captured by ARM_{40mT}/ARM and IRM_{100mT}/IRM_{300mT} have a clear relationship with lower unblocking or alteration temperatures and suppressed Verwey transitions (Figure 8), consistent with these coercivity changes being driven by not just changes in magnetic domain state but also by magnetic mineralogy.

This modern diagenetic environment provides insight into diagenetic processes that likely occurred over the Pleistocene at Site U1538. Thus, in this

framework, ferrimagnetic iron sulfide formation below the base of the SO_4^{2-} reduction zone at around 46 mbsf (~ 33 m ced) at Site U1538 (Figure 2) would represent a horizon where a CRM is acquired in the modern geomagnetic field in sediments that contain an ancient DRM. The depth of this horizon and preservation of these ferrimagnetic iron sulfides likely varies through time as environmental and oceanographic conditions change, but its presence provides a plausible explanation for why the most recent magnetic reversal (the Matuyama-Brunhes) occurs where we expect it to be at Site U1537 (Reilly et al., 2021; Weber et al., 2022), while it is displaced lower by ~ 16 – 22 m at Site U1538 in sediments that have no apparent deformation or other complications (Weber et al., 2021d).

5. Conclusions

Scotia Sea IODP Sites U1537 and U1538 have similar lithostratigraphic but different rock magnetic properties and porewater geochemistry profiles. These observations offer new insights into why Site U1537 has a reliable magnetic polarity signal, but the Site U1538 magnetic polarity stratigraphy is complicated by a poorly defined signal and an apparent ~ 16 – 22 m apparent downward displacement of the most recent geomagnetic reversal (the Matuyama-Brunhes) relative to Site U1537. Rock magnetic property differences suggest at least two ferrimagnetic iron sulfide formation generations at Site U1538. The first generation formed at relatively shallow depths at Site U1538 and seems to be limited to Holocene biogenic diatom oozes. The magnetic signature of these minerals is not as apparent lower in the stratigraphy, which suggests that this generation may be transient in nature near a modern redox boundary and that it is not well preserved in the stratigraphy. The second generation traced by anomalous magnetic mineralogy at Site U1538 relative to Site U1537, formed deeper, at around the 46 m depth of SO_4^{2-} reduction at Site U1538 in the modern and is present below these depths in both diatom-rich interglacial and terrigenous silty-clay glacial sediments. The depth of this horizon is dictated by the porewater geochemistry and may migrate with time as organic carbon supply, sedimentation rate, or other environmental factors vary.

We propose that the presence of Fe^{2+} in porewaters below the SO_4^{2-} reduction zone at Site U1538, but not at Site U1537, creates a geochemical environment favorable for the formation and preservation of authigenic ferrimagnetic iron sulfides that can acquire a CRM at these depths. This geochemical setting can explain the >10 m downward displacement of the Matuyama-Brunhes boundary at Site U1538, where the relative strength of the deep-acquired CRM is similar to or greater than the primary DRM. Where tight stratigraphic control is not available, assessment of porewater geochemistry at other sites globally can provide means to assess the potential of this deep CRM mechanism.

Data Availability Statement

All shipboard generated data can be accessed through the IODP LIMS database (Weber et al., 2021b, 2021c, 2021d; <https://web.iodp.tamu.edu/LORE/>). Magnetic data are available through the MagIC database (Reilly et al., 2024a; Weber et al., 2019). Additional data and rock magnetic data files are available through the Zenodo database (Reilly et al., 2024b).

References

- Amiel, N., Shaar, R., & Sivan, O. (2020). The effect of early diagenesis in methanic sediments on sedimentary magnetic properties: Case study from the SE Mediterranean continental shelf. *Frontiers in Earth Science*, 8, 283. <https://doi.org/10.3389/feart.2020.00283>
- Arndt, J. E., Schenke, H. W., Jakobsson, M., Nitsche, F. O., Buys, G., Goleby, B., et al. (2013). The international bathymetric chart of the Southern Ocean (IBCSO) version 1.0—A new bathymetric compilation covering circum-Antarctic waters. *Geophysical Research Letters*, 40(12), 3111–3117. <https://doi.org/10.1002/grl.50413>
- Bailey, I., Hemming, S., Reilly, B. T., Rollinson, G., Williams, T., Weber, M. E., et al. (2022). Episodes of early Pleistocene West Antarctic ice sheet retreat recorded by Iceberg Alley sediments. *Paleoceanography and Paleoclimatology*, 37(7), e2022PA004433. <https://doi.org/10.1029/2022PA004433>
- Banerjee, S. K., King, J., & Marvin, J. (1981). A rapid method for magnetic granulometry with applications to environmental studies. *Geophysical Research Letters*, 8(4), 333–336. <https://doi.org/10.1029/GL008i004p00333>
- Beal, E. J., House, C. H., & Orphan, V. J. (2009). Manganese- and iron-dependent marine methane oxidation. *Science*, 325(5937), 184–187. <https://doi.org/10.1126/science.1169984>
- Berner, R. A. (1984). Sedimentary pyrite formation: An update. *Geochimica et Cosmochimica Acta*, 48(4), 605–615. [https://doi.org/10.1016/0016-7037\(84\)90089-9](https://doi.org/10.1016/0016-7037(84)90089-9)
- Bilardello, D., & Jackson, M. (2013). What do the Mumpsies do? *The IRM Quarterly*, 23(3). Retrieved from https://drive.google.com/file/d/12ZxZvxIDUyQgx17a-bcrrZrON2DyilQf/view?usp=sharing&usp=embed_facebook
- Blanchet, C. L., Thouveny, N., & Vidal, L. (2009). Formation and preservation of greigite (Fe_3S_4) in sediments from the Santa Barbara Basin: Implications for paleoenvironmental changes during the past 35 ka. *Paleoceanography*, 24(2), PA2224. <https://doi.org/10.1029/2008PA001719>

Acknowledgments

This research used samples and data provided by the International Ocean Discovery Program (IODP). The authors are grateful to the Captain, crew, and IODP staff that made IODP Expedition 382 successful. Part of this work was performed as a Visiting Fellow at the Institute for Rock Magnetism (IRM) at the University of Minnesota. The IRM is a US National Multi-user Facility supported through the Instrumentation and Facilities program of the National Science Foundation, Earth Sciences Division, and by funding from the University of Minnesota. The authors acknowledge support by NSF OPP-ANT Awards 2302832 (B. Reilly), 2114777 (B. Reilly and L. Tauxe), 2114764 (S. Brachfeld), 2114763 (S. Hemming and I. Bailey), and 2114768 (T. Williams) and NSF OCE award 1450528 to the US Science Support Program at Columbia University for post-expedition science activities and its subawards to US members of the IODP Expedition 382 Science Team. L. Tauxe received support from NSF EAR Award 2245628. T. Williams received support from the IODP *JOIDES Resolution* Science Operator (NSF OCE Award 1326927). I. Bailey thanks the Natural Environment Research Council (NERC) for financial support for participation in IODP Exp. 382 and his subsequent research on Site U1538 (UK IODP Grants NE/T006609/1 and NE/T013648/1). M. Weber acknowledges funding by the Deutsche Forschungsgemeinschaft (DFG-Priority Programme 527, Grants We2039/17-2, We2039/19-1). We thank Dr. Andrew Roberts, Dr. Tilo von Dobeneck, and an anonymous reviewer for thoughtful and detailed comments and Dr. Joshua Feinberg for editorial work.

- Canfield, D. E., & Berner, R. A. (1987). Dissolution and pyritization of magnetite in anoxic marine sediments. *Geochimica et Cosmochimica Acta*, 51(3), 645–659. [https://doi.org/10.1016/0016-7037\(87\)90076-7](https://doi.org/10.1016/0016-7037(87)90076-7)
- Channell, J. E. T. (2014). The Iceland Basin excursion: Age, duration, and excursion field geometry. *Geochemistry, Geophysics, Geosystems*, 15(12), 4920–4935. <https://doi.org/10.1002/2014GC005564>
- Channell, J. E. T., Hodell, D. A., Singer, B. S., & Xuan, C. (2010). Reconciling astrochronological and $^{40}\text{Ar}/^{39}\text{Ar}$ ages for the Matuyama-Brunhes boundary and late Matuyama Chron. *Geochemistry, Geophysics, Geosystems*, 11(12), Q0AA12. <https://doi.org/10.1029/2010GC003203>
- Channell, J. E. T., Vázquez Riveiros, N., Gottschalk, J., Waelbroeck, C., & Skinner, L. C. (2017). Age and duration of Laschamp and Iceland basin geomagnetic excursions in the South Atlantic ocean. *Quaternary Science Reviews*, 167, 1–13. <https://doi.org/10.1016/j.quascirev.2017.04.020>
- Chuang, P.-C., Dale, A. W., Heuer, V. B., Hinrichs, K.-U., & Zabel, M. (2021). Coupling of dissolved organic carbon, sulfur and iron cycling in Black Sea sediments over the Holocene and the late Pleistocene: Insights from an empirical dynamic model. *Geochimica et Cosmochimica Acta*, 307, 302–318. <https://doi.org/10.1016/j.gca.2021.04.032>
- Day, R., Fuller, M., & Schmidt, V. A. (1977). Hysteresis properties of titanomagnetites, grain size and compositional dependence. *Physics of the Earth and Planetary Interiors*, 13(4), 260–267. [https://doi.org/10.1016/0031-9201\(77\)90108-x](https://doi.org/10.1016/0031-9201(77)90108-x)
- Diekmann, B., Kuhn, G., Rachold, V., Abelmann, A., Brathauer, U., Fütterer, D. K., et al. (2000). Terrigenous sediment supply in the Scotia Sea (Southern Ocean): Response to Late Quaternary ice dynamics in Patagonia and on the Antarctic Peninsula. *Palaeogeography, Palaeoclimatology, Palaeoecology*, 162(3), 357–387. [https://doi.org/10.1016/S0031-0182\(00\)00138-3](https://doi.org/10.1016/S0031-0182(00)00138-3)
- Dillon, M., & Bleil, U. (2006). Rock magnetic signatures in diagenetically altered sediments from the Niger deep-sea fan. *Journal of Geophysical Research*, 111(B3), B03105. <https://doi.org/10.1029/2004JB003540>
- Ebert, Y., Shaar, R., & Stein, M. (2021). Decadal geomagnetic secular variations from greigite bearing Dead Sea sediments. *Geochemistry, Geophysics, Geosystems*, 22(4), e2021GC009665. <https://doi.org/10.1029/2021GC009665>
- Egli, R. (2013). Variforc: An optimized protocol for calculating non-regular first-order reversal curve (FORC) diagrams. *Global and Planetary Change*, 110(Part C), 302–320. <https://doi.org/10.1016/j.gloplacha.2013.08.003>
- Froelich, P. N., Klinkhammer, G. P., Bender, M. L., Luedtke, N. A., Heath, G. R., Cullen, D., et al. (1979). Early oxidation of organic matter in pelagic sediments of the eastern equatorial Atlantic: Suboxic diagenesis. *Geochimica et Cosmochimica Acta*, 43(7), 1075–1090. [https://doi.org/10.1016/0016-7037\(79\)90095-4](https://doi.org/10.1016/0016-7037(79)90095-4)
- Fu, Y., von Dobeneck, T., Franke, C., Heslop, D., & Kasten, S. (2008). Rock magnetic identification and geochemical process models of greigite formation in Quaternary marine sediments from the Gulf of Mexico (IODP Hole U1319A). *Earth and Planetary Science Letters*, 275(3), 233–245. <https://doi.org/10.1016/j.epsl.2008.07.034>
- Garming, J. F. L., Bleil, U., & Riedinger, N. (2005). Alteration of magnetic mineralogy at the sulfate–methane transition: Analysis of sediments from the Argentine continental slope. *Physics of the Earth and Planetary Interiors*, 151(3–4), 290–308. <https://doi.org/10.1016/j.pepi.2005.04.001>
- Gradstein, F. M., Ogg, J., Schmitz, M., & Ogg, G. (Eds.) (2012). *The geologic time scale 2012* (1st ed.). Elsevier.
- Haeckel, E. (1861). *Abbildungen und Diagnosen neuer Gattungen und Arten von lebenden Radiolarien des Mittelmeeres* (pp. 834–845). Monatsberichte Der Königlichen Akademie Der Wissenschaften Zu Berlin.
- Harrison, R. J., & Feinberg, J. M. (2008). FORCinel: An improved algorithm for calculating first-order reversal curve distributions using locally weighted regression smoothing. *Geochemistry, Geophysics, Geosystems*, 9(5), Q05016. <https://doi.org/10.1029/2008GC001987>
- Harrison, R. J., Muraszko, J., Heslop, D., Lascu, I., Muxworthy, A. R., & Roberts, A. P. (2018). An improved algorithm for unmixing first-order reversal curve diagrams using principal component analysis. *Geochemistry, Geophysics, Geosystems*, 19(5), 1595–1610. <https://doi.org/10.1029/2018GC007511>
- Hays, J. D., & Opdyke, N. D. (1967). Antarctic radiolaria, magnetic reversals, and climatic change. *Science*, 158(3804), 1001–1011. <https://doi.org/10.1126/science.158.3804.1001>
- Hornig, C.-S. (2018). Unusual magnetic properties of sedimentary pyrrhotite in methane seepage sediments: Comparison with metamorphic pyrrhotite and sedimentary greigite. *Journal of Geophysical Research: Solid Earth*, 123(6), 4601–4617. <https://doi.org/10.1002/2017JB015262>
- Hornig, C.-S., & Roberts, A. P. (2018). The low-temperature Besnus magnetic transition: Signals due to monoclinic and hexagonal pyrrhotite. *Geochemistry, Geophysics, Geosystems*, 19(9), 3364–3375. <https://doi.org/10.1029/2017GC007394>
- Hunger, S., & Benning, L. G. (2007). Greigite: A true intermediate on the polysulfide pathway to pyrite. *Geochemical Transactions*, 8(1), 1. <https://doi.org/10.1186/1467-4866-8-1>
- Jiang, W.-T., Hornig, C.-S., Roberts, A. P., & Peacor, D. R. (2001). Contradictory magnetic polarities in sediments and variable timing of neof ormation of authigenic greigite. *Earth and Planetary Science Letters*, 193(1), 1–12. [https://doi.org/10.1016/S0012-821X\(01\)00497-6](https://doi.org/10.1016/S0012-821X(01)00497-6)
- Kao, S.-J., Hornig, C.-S., Roberts, A. P., & Liu, K.-K. (2004). Carbon–sulfur–iron relationships in sedimentary rocks from southwestern Taiwan: Influence of geochemical environment on greigite and pyrrhotite formation. *Chemical Geology*, 203(1–2), 153–168. <https://doi.org/10.1016/j.chemgeo.2003.09.007>
- Karlin, R., & Levi, S. (1983). Diagenesis of magnetic minerals in recent hemipelagic sediments. *Nature*, 303(5915), 327–330. <https://doi.org/10.1038/303327a0>
- King, J., Banerjee, S. K., Marvin, J., & Özdemir, Ö. (1982). A comparison of different magnetic methods for determining the relative grain size of magnetite in natural materials: Some results from lake sediments. *Earth and Planetary Science Letters*, 59(2), 404–419. [https://doi.org/10.1016/0012-821X\(82\)90142-X](https://doi.org/10.1016/0012-821X(82)90142-X)
- Liu, J., Zhu, R., Roberts, A. P., Li, S., & Chang, J.-H. (2004). High-resolution analysis of early diagenetic effects on magnetic minerals in post-middle-Holocene continental shelf sediments from the Korea Strait. *Journal of Geophysical Research*, 109(B3). <https://doi.org/10.1029/2003JB002813>
- Liu, Q., Roberts, A. P., Larrasoña, J. C., Banerjee, S. K., Guyodo, Y., Tauxe, L., & Oldfield, F. (2012). Environmental magnetism: Principles and applications. *Reviews of Geophysics*, 50(4), RG4002. <https://doi.org/10.1029/2012RG000393>
- Lowrie, W. (1990). Identification of ferromagnetic minerals in a rock by coercivity and unblocking temperature properties. *Geophysical Research Letters*, 17(2), 159–162. <https://doi.org/10.1029/GL017i002p00159>
- Matsuoka, K., Skoglund, A., Roth, G., de Pomereu, J., Griffiths, H., Headland, R., et al. (2021). Quantarctica, an integrated mapping environment for Antarctica, the Southern Ocean, and sub-Antarctic islands. *Environmental Modelling & Software*, 140, 105015. <https://doi.org/10.1016/j.envsoft.2021.105015>
- Moskowitz, B. M., Frankel, R. B., & Bazylinski, D. A. (1993). Rock magnetic criteria for the detection of biogenic magnetite. *Earth and Planetary Science Letters*, 120(3), 283–300. [https://doi.org/10.1016/0012-821X\(93\)90245-5](https://doi.org/10.1016/0012-821X(93)90245-5)
- Nowaczyk, N., Frank, U., Kind, J., & Arz, H. W. (2013). A high-resolution paleointensity stack of the past 14 to 68 ka from Black Sea sediments. *Earth and Planetary Science Letters*, 384, 1–16. <https://doi.org/10.1016/j.epsl.2013.09.028>

- Opdyke, N. D., Glass, B., Hays, J. D., & Foster, J. (1966). Paleomagnetic study of Antarctic deep-sea cores. *Science*, *154*(3747), 349–357. <https://doi.org/10.1126/science.154.3747.349>
- Peck, V. L., Weber, M. E., Raymo, M. E., Williams, T., Armbrrecht, L., Bailey, I., et al. (2021). Site U1534. In *Volume 382: Iceberg Alley and subantarctic ice and ocean dynamics* (Vol. 382). International Ocean Discovery Program. <https://doi.org/10.14379/iodp.proc.382.103.2021>
- Pérez, L. F., Martos, Y. M., García, M., Weber, M. E., Raymo, M. E., Williams, T., et al. (2021). Miocene to present oceanographic variability in the Scotia Sea and Antarctic ice sheets dynamics: Insight from revised seismic-stratigraphy following IODP Expedition 382. *Earth and Planetary Science Letters*, *553*, 116657. <https://doi.org/10.1016/j.epsl.2020.116657>
- Peters, C., & Thompson, R. (1998). Magnetic identification of selected natural iron oxides and sulphides. *Journal of Magnetism and Magnetic Materials*, *183*(3), 365–374. [https://doi.org/10.1016/S0304-8853\(97\)01097-4](https://doi.org/10.1016/S0304-8853(97)01097-4)
- Pike, C. R., Roberts, A. P., & Verosub, K. L. (1999). Characterizing interactions in fine magnetic particle systems using first order reversal curves. *Journal of Applied Physics*, *85*(9), 6660–6667. <https://doi.org/10.1063/1.370176>
- Poullton, S. W., Krom, M. D., & Raiswell, R. (2004). A revised scheme for the reactivity of iron (oxyhydr)oxide minerals towards dissolved sulfide. *Geochimica et Cosmochimica Acta*, *68*(18), 3703–3715. <https://doi.org/10.1016/j.gca.2004.03.012>
- Pugh, R. S., McCave, I. N., Hillenbrand, C.-D., & Kuhn, G. (2009). Circum-Antarctic age modelling of Quaternary marine cores under the Antarctic Circumpolar Current: Ice-core dust–magnetic correlation. *Earth and Planetary Science Letters*, *284*(1), 113–123. <https://doi.org/10.1016/j.epsl.2009.04.016>
- Reilly, B., Tauxe, L., Brachfeld, S., Kenlee, B., Gutjahr, M., Andrew, D. W., et al. (2024a). A geochemical mechanism for >10 m offsets of magnetic reversals inferred from the comparison of two Scotia Sea drill sites (Version 1) [Dataset]. *Magnetics Information Consortium (MagIC)*. <https://doi.org/10.7288/V4/MAGIC/19778>
- Reilly, B., Tauxe, L., Brachfeld, S., Kenlee, B., Gutjahr, M., Andrew, D. W., et al. (2024b). Rock magnetic data from IODP Exp. 382 Sites U1537 and U1538 to support Reilly et al. “A geochemical mechanism for >10 m offsets of magnetic reversals inferred from the comparison of two Scotia Sea drill sites” (Version v1) [Dataset]. *Zenodo*. <https://doi.org/10.5281/zenodo.10035107>
- Reilly, B. T., McCormick, M. L., Brachfeld, S. A., & Haley, B. A. (2020). Authigenic ferrimagnetic iron sulfide preservation due to nonsteady state diagenesis: A perspective from Perseverance Drift, Northwestern Weddell Sea. *Geochemistry, Geophysics, Geosystems*, *21*(11), e2020GC009380. <https://doi.org/10.1029/2020GC009380>
- Reilly, B. T., Tauxe, L., Brachfeld, S., Raymo, M., Bailey, I., Hemming, S., et al. (2021). New magnetostratigraphic insights From Iceberg Alley on the rhythms of Antarctic climate during the Plio-Pleistocene. *Paleoceanography and Paleoclimatology*, *36*(2), e2020PA003994. <https://doi.org/10.1029/2020PA003994>
- Reynolds, R. L., Rosenbaum, J. G., van Metre, P., Tuttle, M., Callender, E., & Goldin, A. (1999). Greigite (Fe₃S₄) as an indicator of drought—The 1912–1994 sediment magnetic record from White Rock Lake, Dallas, Texas, USA. *Journal of Paleolimnology*, *21*(2), 193–206. <https://doi.org/10.1023/A:1008027815203>
- Richter, C., Acton, G., Endris, C., & Radsted, M. (2007). Handbook for shipboard paleomagnetists. In *ODP technical note, 34*. Retrieved from http://www-odp.tamu.edu/Publications/notes/tn34/tn34_.htm
- Riedinger, N., Formolo, M. J., Lyons, T. W., Henkel, S., Beck, A., & Kasten, S. (2014). An inorganic geochemical argument for coupled anaerobic oxidation of methane and iron reduction in marine sediments. *Geobiology*, *12*(2), 172–181. <https://doi.org/10.1111/gbi.12077>
- Roberts, A. P. (2015). Magnetic mineral diagenesis. *Earth-Science Reviews*, *151*, 1–47. <https://doi.org/10.1016/j.earscirev.2015.09.010>
- Roberts, A. P., Chang, L., Rowan, C. J., Horng, C.-S., & Florindo, F. (2011). Magnetic properties of sedimentary greigite (Fe₃S₄): An update. *Reviews of Geophysics*, *49*(1). <https://doi.org/10.1029/2010RG000336>
- Roberts, A. P., Pike, C. R., & Verosub, K. L. (2000). First-order reversal curve diagrams: A new tool for characterizing the magnetic properties of natural samples. *Journal of Geophysical Research*, *105*(B12), 28461–28475. <https://doi.org/10.1029/2000jb900326>
- Roberts, A. P., & Weaver, R. (2005). Multiple mechanisms of remagnetization involving sedimentary greigite (Fe₃S₄). *Earth and Planetary Science Letters*, *231*(3), 263–277. <https://doi.org/10.1016/j.epsl.2004.11.024>
- Roberts, A. P., Zhao, X., Harrison, R. J., Heslop, D., Muxworthy, A. R., Rowan, C. J., et al. (2018). Signatures of reductive magnetic mineral diagenesis from unmixing of first-order reversal curves. *Journal of Geophysical Research: Solid Earth*, *123*(6), 4500–4522. <https://doi.org/10.1029/2018JB015706>
- Robinson, S. G. (1986). The late Pleistocene palaeoclimatic record of North Atlantic deep-sea sediments revealed by mineral-magnetic measurements. *Physics of the Earth and Planetary Interiors*, *42*(1), 22–47. [https://doi.org/10.1016/S0031-9201\(86\)80006-1](https://doi.org/10.1016/S0031-9201(86)80006-1)
- Rowan, C. J., Roberts, A. P., & Broadbent, T. (2009). Reductive diagenesis, magnetite dissolution, greigite growth and paleomagnetic smoothing in marine sediments: A new view. *Earth and Planetary Science Letters*, *277*(1–2), 223–235. <https://doi.org/10.1016/j.epsl.2008.10.016>
- Shackleton, N. J., & Opdyke, N. D. (1973). Oxygen isotope and palaeomagnetic stratigraphy of Equatorial Pacific core V28-238: Oxygen isotope temperatures and ice volumes on a 10⁵ year and 10⁶ year scale. *Quaternary Research*, *3*(1), 39–55. [https://doi.org/10.1016/0033-5894\(73\)90052-5](https://doi.org/10.1016/0033-5894(73)90052-5)
- Snowball, I., & Thompson, R. (1990). A stable chemical remanence in Holocene sediments. *Journal of Geophysical Research*, *95*(B4), 4471–4479. <https://doi.org/10.1029/JB095iB04p04471>
- Sprenk, D., Weber, M. E., Kuhn, G., Rosén, P., Frank, M., Molina-Kescher, M., et al. (2013). Southern Ocean bioproductivity during the last glacial cycle—New detection method and decadal-scale insight from the Scotia Sea. *Geological Society, London, Special Publications*, *381*(1), 245–261. <https://doi.org/10.1144/SP381.17>
- Stephenson, A. (1993). Three-axis static alternating field demagnetization of rocks and the identification of natural remanent magnetization, gyroremanent magnetization, and anisotropy. *Journal of Geophysical Research*, *98*(B1), 373–381. <https://doi.org/10.1029/92JB01849>
- Stober, J. C., & Thompson, R. (1979). An investigation into the source of magnetic minerals in some Finnish lake sediments. *Earth and Planetary Science Letters*, *45*(2), 464–474. [https://doi.org/10.1016/0012-821X\(79\)90145-6](https://doi.org/10.1016/0012-821X(79)90145-6)
- Tauxe, L., Herbert, T., Shackleton, N. J., & Kok, Y. S. (1996). Astronomical calibration of the Matuyama-Brunhes boundary: Consequences for magnetic remanence acquisition in marine carbonates and the Asian loess sequences. *Earth and Planetary Science Letters*, *140*(1–4), 133–146. [https://doi.org/10.1016/0012-821X\(96\)00030-1](https://doi.org/10.1016/0012-821X(96)00030-1)
- Warnock, J. P., Reilly, B. T., Raymo, M. E., Weber, M. E., Peck, V., Williams, T., et al. (2022). Latitudinal variance in the drivers and pacing of warmth during Mid-Pleistocene MIS 31 in the Antarctic zone of the Southern Ocean. *Paleoceanography and Paleoclimatology*, *37*(8), e2021PA004394. <https://doi.org/10.1029/2021PA004394>
- Weber, M. E., Bailey, I., Hemming, S. R., Martos, Y. M., Reilly, B. T., Ronge, T. A., et al. (2022). Antiphased dust deposition and productivity in the Antarctic Zone over 1.5 million years. *Nature Communications*, *13*(1), 1–18. <https://doi.org/10.1038/s41467-022-29642-5>
- Weber, M. E., Kuhn, G., Sprenk, D., Rolf, C., Ohlwein, C., & Ricken, W. (2012). Dust transport from Patagonia to Antarctica—A new stratigraphic approach from the Scotia Sea and its implications for the last glacial cycle. *Quaternary Science Reviews*, *36*, 177–188. <https://doi.org/10.1016/j.quascirev.2012.01.016>

- Weber, M. E., Raymo, M. E., Peck, V. L., & Williams, T. (2019). Expedition 382 Preliminary Report: Iceberg Alley and subantarctic ice and ocean dynamics (version 1) [Dataset]. *Magnetics Information Consortium (MagIC)*. <https://doi.org/10.7288/V4/MAGIC/16842>
- Weber, M. E., Raymo, M. E., Peck, V. L., Williams, T., Armbrrecht, L., Bailey, I., et al. (2021a). Expedition 382 methods. In *Volume 382: Iceberg Alley and subantarctic ice and ocean dynamics* (Vol. 382). International Ocean Discovery Program. <https://doi.org/10.14379/iodp.proc.382.102.2021>
- Weber, M. E., Raymo, M. E., Peck, V. L., Williams, T., Armbrrecht, L., Bailey, I., et al. (2021b). Expedition 382 summary. In *Volume 382: Iceberg Alley and subantarctic ice and ocean dynamics* (Vol. 382). International Ocean Discovery Program. <https://doi.org/10.14379/iodp.proc.382.101.2021>
- Weber, M. E., Raymo, M. E., Peck, V. L., Williams, T., Armbrrecht, L., Bailey, I., et al. (2021c). Site U1537. In *Volume 382: Iceberg Alley and subantarctic ice and ocean dynamics* (Vol. 382). International Ocean Discovery Program. <https://doi.org/10.14379/iodp.proc.382.106.2021>
- Weber, M. E., Raymo, M. E., Peck, V. L., Williams, T., Armbrrecht, L., Bailey, I., et al. (2021d). Site U1538. In *Volume 382: Iceberg Alley and subantarctic ice and ocean dynamics* (Vol. 382). International Ocean Discovery Program. <https://doi.org/10.14379/iodp.proc.382.107.2021>
- Xiao, W., Frederichs, T., Gersonde, R., Kuhn, G., Esper, O., & Zhang, X. (2016). Constraining the dating of late Quaternary marine sediment records from the Scotia Sea (Southern Ocean). *Quaternary Geochronology*, *31*(Supplement C), 97–118. <https://doi.org/10.1016/j.quageo.2015.11.003>
- Yamazaki, T., Abdeldayem, A. L., & Ikehara, K. (2003). Rock-magnetic changes with reduction diagenesis in Japan Sea sediments and preservation of geomagnetic secular variation in inclination during the last 30,000 years. *Earth Planets and Space*, *55*(6), 327–340. <https://doi.org/10.1186/BF03351766>
- Zijderveld, J. D. A. (1967). AC demagnetization of rocks: Analysis of results. In *Methods in paleomagnetism* (Vol. 1, pp. 254–286). <https://doi.org/10.1016/b978-1-4832-2894-5.50049-5>